Sm3+/Gd3+ Co-doped Lead/Bismuth Borogermanate Glasses – New Materials for Luminescent Thermometry

Sofia Zykova , Kristina Runina * , Igor Avetissov * , Ksenia Serkina , Olga Petrova , Kirill N. Boldyrev

Posted Date: 4 January 2024

doi: 10.20944/preprints202401.0267.v1

Keywords: glass; boron oxide; germanium oxide; lead oxide; bismuth oxide; rare earth ions; luminescence; thermoluminescence

Article

Sm^{3+}/Gd^{3+} Co-Doped Lead/Bismuth Borogermanate Glasses—New Materials for Luminescent Thermometry

Sofia Zykova [1], Ksenia Serkina [1], Kristina Runina [1,*], Olga Petrova [1], Igor Avetissov [1,*] and Kirill Boldyrev [2]

[1] Department of Chemistry and Technology of Crystals, D. Mendeleev University of Chemical Technology of Russia (MUCTR), Moscow 125480, Russia; avetisov.i.k@muctr.ru

[2] Laboratory of Fourier-spectroscopy, Institute for Spectroscopy RAS, Troitsk, Russia

* Correspondence: runinakristina@mail.ru; igor_avetisov@mail.ru

Abstract: The Sm^{3+}/Gd^{3+} co-doped glasses in the B_2O_3–GeO_2–PbO and B_2O_3–GeO_2–Bi_2O_3 systems have been synthesized in the composition range of $40B_2O_3$–$40GeO_2$–(15-17)PbO(Bi_2O_3)–(3-2)Sm_2O_3–(2-1)Gd_2O_3 and $42.5B_2O_3$–$42.5GeO_2$–(11.25-12.75)PbO(Bi_2O_3)–(2.25-1.5)Sm_2O_3–(1.5-0.075)Gd_2O_3. The physical, structural, and spectral properties of the produced glasses have been studied. The fabricated glass samples demonstrated changes in temperature-sensitive luminescence parameters in 298-673 K temperature range. We found out several photoluminescence bands attributed with transitions from different Stark sublevels of Sm^{3+}. By using a combination of two temperature sensitive and one non-sensitive transitions we calculated fluorescence intensities ratio (FIR). This procedure made it possible to increase the sensitivity of luminescence thermometry in several times. Such method could be very useful for the luminescent thermometry materials based on Ln^{3+} ions with multiplied *f-f* transitions. The most remarkable temperature-sensitive luminescent parameter for the Pb-based glasses has occurred to be the luminescence intensity, which reduced in 1.5 time, while for the Bi-based glasses it was the modified luminescence intensity ratio between several bands. The results showed that the produced glasses are perspective for luminescence thermometry.

Keywords: glass; boron oxide; germanium oxide; lead oxide; bismuth oxide; rare earth ions; luminescence; thermoluminescence

1. Introduction

Temperature (T) is one of the most fundamental parameter in all technological processes. Thermosensors are widely used in metrology, environment, high-temperature engineering, chemistry, medicine, biology, physiology, air conditioning, in production plants and the storage of goods etc. T-sensors are estimated to fill as much as 75–80% of the world's sensor market [1]. The first wide spread types of thermometers were liquid-filled glass thermometers [2]. In the 19th century, the real breakthrough in thermometry was made using the Seebeck effect, which gave rise to the era of thermocouples. The next step in thermometry dealt with optical sensors of various types [3], which cross the threshold of 3700 K and made it possible to apply the thermometry in plasma technologies.

In the last 20 years, there has been growing interest in luminescent thermometry (LT), due to its higher efficiency in accurately measuring the temperature of objects with sizes less than 10 μm [4], fast response, high thermal and spatial resolution, as well as a wide range of operating temperatures from 10 K up to 1300 K [5]. Luminescence thermometry can operate in extremely high electric fields [6], unlike thermocouples. This opens up opportunities for its application in industry [7], scientific research [8] and biomedicine [9]. However, in recent decades, the most popular LT temperature range has been the measurement of physiological temperature over a narrow temperature range of 300–330 K with high spatial resolution and accuracy better than 0.1 °C.

There are many scientific applications that require fast sensing with high spatial resolution, unaffected by strong electromagnetic fields, in the temperature range from RT to 673 K and above.

Preprints (www.preprints.org) | NOT PEER-REVIEWED | Posted: 4 January 2024 doi:10.20944/preprints202401.0267.v1

For example, for studying heat and mass transfer in liquids in various technological and chemical processes, measuring local temperature is very important. Correct 3D mapping of temperature inside chemical reactors in which processes occur during ultrasonic or microwave activation is a very urgent task for substantiating a numerical model of the technological process. This problem could only be solved using fluorescent thermometry. Sometimes, in order to develop a correct numerical model for the growth of crystals from a melt at high temperatures (1000-3000 K) [10], information on 3D temperature mapping in the volume of the melt is very important to correct the growth process. To solve the problem, scientists use numerical modeling, which requires confirmation by physical experiments at relatively low temperatures [11]. The application of LT for 3D temperature mapping of melt volume is a promising tool for improving numerical models.

Over the decades, two classes of methods: time-resolved methods and spectral-resolved methods, using both emission lifetimes and spectral responses, have found application in remote thermometry.

Temperature determination through LT can be based on monitoring various photoluminescence (PL) temperature-sensitive parameters [12–14], including absolute PL intensity (Figure 1a), spectral width of the PL band (Figure 1b), fluorescence intensity ratio of two bands (FIR) (Figure 1c), spectral shift of the PL band maximum (Figure 1d), and excited-state lifetime (Figure 1e).

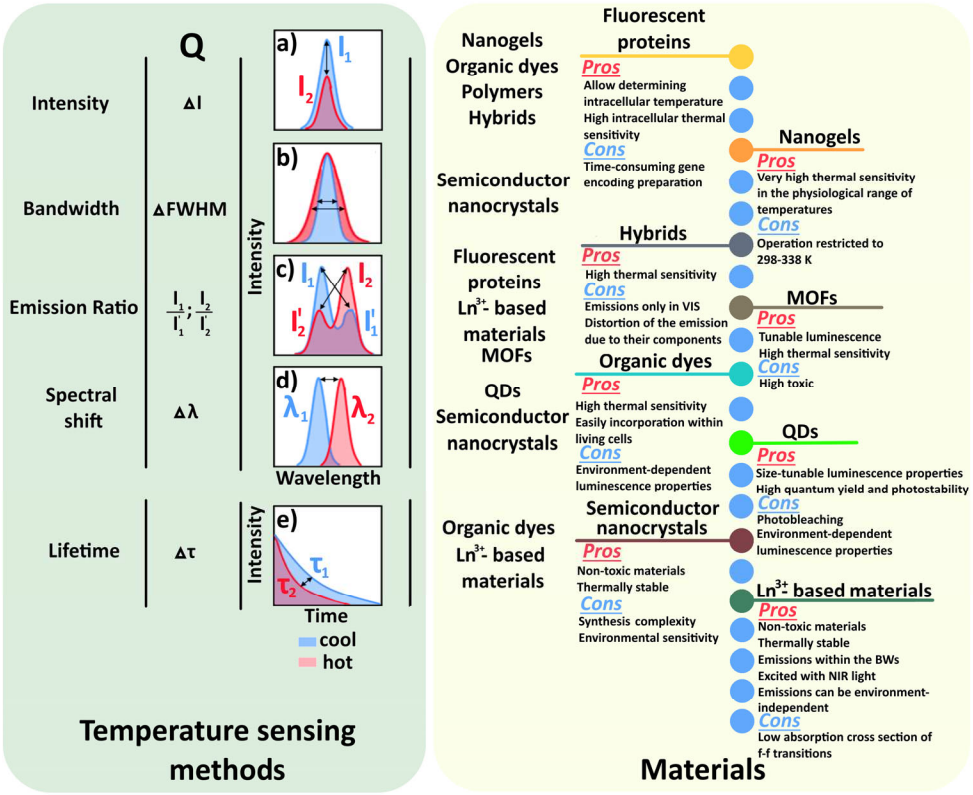

Figure 1. Schematic representation of the possible effects caused by a temperature increment on the luminescence (left) and corresponding materials using in the luminescent thermometry (right).

LT does not provide the value of the temperature directly; instead, it provides an indication (Q). Depending on Q the luminescent thermometry is classified as fluorescent intensity thermometry, imaging luminescent thermometry, fluorescent intensity ratio thermometry (FIR), luminescent decay time thermometry.

The most important parameters to quantifying measurement performance are the measurement temperature range, absolute (S_a) and relative (S_r) sensitivities, temperature resolution (δT), temporal resolution (δx_{min}), spatial resolution (δt_{min}), the repeatability and reproducibility (R).

Preprints (www.preprints.org) | NOT PEER-REVIEWED | Posted: 4 January 2024 doi:10.20944/preprints202401.0267.v1

$$S_a = \left|\frac{dQ}{dT}\right|, \quad (1)$$

$$S_r = \left|\frac{1}{Q} \times \frac{dQ}{dT}\right| \times 100\%, \quad (2)$$

$$\delta T = \frac{\sigma}{S_a} = \frac{\sigma_r}{S_r}, \quad (3)$$

$$\delta x_{min} = \frac{\delta T}{|dT/dx|}, \quad (4)$$

$$\delta t_{min} = \frac{\delta T}{|dT/dt|}, \quad (5)$$

$$R = 1 - \frac{max|\bar{Q} - Q_1|}{Q} \quad (6)$$

The advantages of LT are high sensitivity, independence of the measured quantity from absolute value of PL intensities and excitation energy [15]. From the technical point of view, FIR could be easy implemented by comparing the intensities of only selected bands using narrowband filters and sensitive semiconducting detectors.

A variety of materials both well-ordered such as inorganic single crystals and strongly disordered such as organic dyes as well as nanostructured materials such as nanogels and quantum dots are used for sensitive elements of luminescent thermometers.

Among the luminescent materials investigated as potential LT sensors, special attention is given to materials doped with lanthanides due to their non-toxicity, thermal stability, high quantum yield, and emission independence from matrix [16]. In LT materials co-doped with different Ln^{3+} ions, e.g., Eu^{3+} and Tb^{3+}, the ions are binding between each other and energy-transfer from excited levels may followed by a strong temperature dependence [5,17,18]. This mechanism does not lead to thermal equilibrium of populations in the excited state, which makes possible higher relative sensitivity if the luminescence intensity of various ions is sufficient enough [19,20]. The operating mechanism of energy transfer luminescent thermometers is complex because it depends not only on relaxation processes within the ion, but also involves interactions between different ions as well as the influence of the crystal field of the matrix.

Metalorganic Ln-ion based on β-diketonate chelates demonstrated S_r=4,9 %×K^{-1} in the 10-350 K temperature range [5]. High temperature LT sensors based on YAG:Dy and YAG:Dy, Er single crystals [21] performed an excellent S_r=0,9 %×K^{-1} in the temperature range up to 1973 K.

Optical quality glasses (contains commonly network former, intermediates, and modifiers) are considered a cheap alternative for creation a uniform doped compact material with adjustable PL, mechanical and chemical properties. For the last decade there were published a number of articles on the problem of functional glasses in the systems of B_2O_3-PbO-Bi_2O_3-GeO_2 [22], Bi_2O_3-GeO_2 [23], and B_2O_3-GeO_2-Gd_2O_3 [24], doped with Sm^{3+} and/or Gd^{3+}. The above investigations have proved the perspective of such glasses application as orange lighting sources [25] and key-feature components of optoelectronic devices [26]. Nevertheless, for LT application B_2O_3-PbO-Bi_2O_3-GeO_2 glasses doped by RE has not been reported yet.

In this study, we have investigated for the first time luminescent properties of glasses in the systems of B_2O_3–GeO_2–PbO and B_2O_3–GeO_2–Bi_2O_3 co-doped by Sm^{3+}/Gd^{3+} *vs* temperature. Particular attention was paid to the search for a new function to increase the sensitivity of LT materials.

 doi:10.20944/preprints202401.0267.v1

2. Materials and Methods

2.1. Materials and synthesis

We used Bi_2O_3 99.999 wt%, GeO_2 99.995 wt% (LANHIT LTD, Moscow, Russia), PbO 99.5 wt%, B_2O_3 98.5 wt% (Khimkraft, Kaliningrad, Russia), Sm_2O_3 99,9 wt%, Gd_2O_3 99.9 wt% (POLARIT LTD, Moscow, Russia). We synthesized glasses with the general formulas $40B_2O_3$–$40GeO_2$–x$PbO(Bi_2O_3)$–ySm_2O_3–zGd_2O_3, where x = 15, 16, 17; y = 3, 2.5, 2; z = 2, 1.5, 1 mol% and $42.5B_2O_3$–$42.5GeO_2$–x$PbO(Bi_2O_3)$–ySm_2O_3–zGd_2O_3, where x = 11.25, 12, 12.75; y = 2.25, 1.875, 1.5; z = 1.5, 1.125, 0.075 mol%.

For the easy presentation of the results, we made the following notation of the glass samples (see Table 1).

Table 1. Notations (sample ID) of the glasses under study.

Sample ID /Notation	Glass composition (mol.%)	Sample ID /Notation	Glass composition (mol.%)
(12.75)Pb(1.5)Sm (0.75)Gd-42.5	$42.5B_2O_3$–$42.5GeO_2$–12.75PbO–$1.5Sm_2O_3$–$0.75Gd_2O_3$	**(12.75)Bi(1.5)Sm (0.75)Gd-42.5**	$42.5B_2O_3$–$42.5GeO_2$–$12.75Bi_2O_3$–$1.5Sm_2O_3$–$0.75Gd_2O_3$
(12)Pb (1.875)Sm (1.125)Gd-42.5	$42.5B_2O_3$–$42.5GeO_2$–12PbO–$1.875Sm_2O_3$–$1.125Gd_2O_3$	**(12)Bi(1.875)Sm (1.125)Gd-42.5**	$42.5B_2O_3$–$42.5GeO_2$–$12Bi_2O_3$–$1.875Sm_2O_3$–$1.125Gd_2O_3$
(11.25)Pb (2.25)Sm (1.5)Gd-42.5	$42.5B_2O_3$–$42.5GeO_2$–11.25PbO–$2.25Sm_2O_3$–$1.5Gd_2O_3$	**(11.25)Bi(2.25)Sm (1.5)Gd-42.5**	$42.5B_2O_3$–$42.5GeO_2$–$11.25Bi_2O_3$–$2.25Sm_2O_3$–$1.5Gd_2O_3$
(17)Pb(2.0)Sm (1.0)Gd-40	$40B_2O_3$–$40GeO_2$–17PbO–$2Sm_2O_3$–$1Gd_2O_3$	**(17)Bi(2.0)Sm (1.0)Gd-40**	$40B_2O_3$–$40GeO_2$–$17Bi_2O_3$–$2Sm_2O_3$–$1Gd_2O_3$
(16)Pb(2.5)Sm (1.5)Gd-40	$40B_2O_3$–$40GeO_2$–16PbO–$2.5Sm_2O_3$–$1.5Gd_2O_3$	**(16)Bi(2.5)Sm (1.5)Gd-40**	$40B_2O_3$–$40GeO_2$–$16Bi_2O_3$–$2.5Sm_2O_3$–$1.5Gd_2O_3$
(15)Pb(3.0)Sm (2.0)Gd-40	$40B_2O_3$–$40GeO_2$–15PbO–$3Sm_2O_3$–$2Gd_2O_3$	**(15)Bi(3.0)Sm (2.0)Gd-40**	$40B_2O_3$–$40GeO_2$–$15Bi_2O_3$–$3Sm_2O_3$–$2Gd_2O_3$

Glasses were synthesized in corundum crucibles at 1373 K for 30 min by the standard melt-quenching technique with casting onto a glassy carbon substrate at room temperature. Thermal stresses were removed by annealing at 573 K for 3 h, followed by cooling at ~100 K/h rate. Polished plane-parallel plates with 1.8 mm thickness were fabricated from glasses for further studies.

2.2. Characterization techniques

Structure analysis

The glass samples were grinded to 20 μm powder and their structure was examined by X-ray diffraction using an Equinox-2000 diffractometer (Inel SAS, Artnay, France) with CuKα radiation (λ=1.54056 Å). The element analysis of the synthesized glasses was carried out using X-ray spectral energy-dispersive microanalyzer (EDS Oxford Instruments X-MAX-50, Abingdon, Oxfordshire, UK) on the base of Tescan VEGA3-LMU scanning electron microscope (TESCAN ORSAY HOLDING, Brno, Czech Republic).

Raman spectra were recorded on a QE65000 spectrophotometer (Ocean Optics, Largo, FL, USA) using a 785 nm excitation laser in the frequency shift range of 200–2000 cm^{-1} in backscattering geometry. FT-IR absorption spectra were recorded on a Tensor 27 IR-Fourier spectrometer (Bruker, Ettlingen, Germany) in 400–8000 cm^{-1} range.

Glass characterization

The glass transition temperatures of the samples were determined by differential scanning calorimetry methods using a NETZSCH STA 449 F3 Jupiter instrument (Erich Netzsch GmbH & Co. Holding KG, Selb, Germany) with 1 K accuracy. The measurements were carried out for 15 mg bulk

 doi:10.20944/preprints202401.0267.v1

samples placed in platinum crucibles at 10 K/min heating rate. The density of the samples was determined by the hydrostatic method using a MER123 ACF JR-150.005 TFT balance (Mercury WP Tech Group Co., Ltd., Incheon, The Republic of Korea) with the accuracy of 0.005 g/cm^3.

Optical characterization techniques

The refractive index was determined using a MEGEON 72022 gemological refractometer (MEGEON, Moscow, Russia) with 1.78 refractive index liquid (sample $n_D < 1.78$) and a MIN-8 optical microscope (LOMO JSC, Saint Peterburg, Russia) by measuring the shift of the refracted beam at different preset tilt angles of sample plates located on a special stage (sample $n_D > 1.78$). The measuring accuracy was 0.01.

The absorption spectra were recorded on a JASCO V-770 spectrophotometer (JASCO Corporation, Tokyo, Japan) in the 190–2700 nm wavelength range with 1 nm step.

The photoluminescence and excitation spectra at room temperature were recorded on an Fluorolog FL3-22 (Horiba Jobin Yvon, Longjumeau, France) with double monohromatization of both excitation and emission radiation in 400–720 nm wavelength range with 1 nm step; the PL decay kinetics were measured on a Fluorolog FL3-22 (Horiba Jobin Yvon, Longjumeau, France) with 370 nm a pulsed diode excitation and $\Delta\tau = 1.5$ ns. The decay kinetics was carried out using the OriginPro 8 SR4 program (OriginLab Corp., Northampton, MA, USA) using the Fit Exponential procedure.

The thermoluminescence spectra were recorded on an OpticInsight OCEAN-HDX-UV-VIS fiber optic spectrometer (Ocean Insight, Orlando, FL, USA) under excitation with an XML T6 10W 365 nm laser LED (TiaoChongYi, Changchun, China). Heating and cooling of glass samples were carried out using Optical cryo and high temperature stage (SIMTRUM Pte. Ltd., Singapore, Singapore) with temperature control range from room temperature to 673 K.

In all PL measurements the exciting beam spot was 0.5 mm.

3. Experimental results

3.1. Glass samples

Pb-based glasses have a pale-yellow color, which is attributed to the presence of lead oxide (Figure 2). Pb-based glasses with a matrix composition of 40–40 have a more intense yellow color, due to an increase in the content of lead oxide shifts the short-wavelength absorption edge to the long-wavelength region of the spectrum [27].

Bi-based glasses had a ruby-red color due to the absorption shoulder in the region of 500 nm attributed with bismuth active centers [28], which becomes more saturated at bismuth oxide content increase.

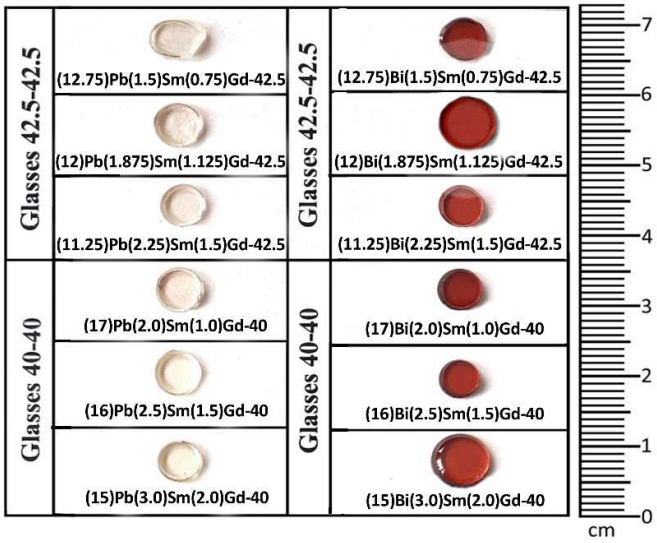

Figure 2. The photographs of B_2O_3–GeO_2–PbO and B_2O_3–GeO_2–Bi_2O_3 glasses co-doped by Sm^{3+}/Gd^{3+}.

Preprints (www.preprints.org) | NOT PEER-REVIEWED | Posted: 4 January 2024 doi:10.20944/preprints202401.0267.v1

The results of the elemental analysis (XFS-EDS) of the glasses showed that all samples were characterized by homogeneous composition and all of them contained an aluminum impurity due to the synthesis in corundum crucibles, which was explained by the chemical action of fluid PbO or Bi_2O_3 with the crucible material (for details see Figure S31-S42 and Table S1).

3.2. Glass structure characterisation

X-ray diffraction patterns of all synthesized glasses demonstrated a wide halo in 21-36 degree 2θ range (Figure S1) which proved the amorphous nature of all glass samples.

Samples of the two systems under consideration have common vibron modes in all frequency regions of Raman spectra (Figure S2-S3) and the corresponding interpretations are presented in Table 2, which correlates with various literature data.

In the low-frequency range (300–700 cm^{-1}) we observed a band in the 460-465 cm^{-1} range which was referred to the symmetrical stretching of Ge–O–Ge bonds in 4- or 6-membered Ge^{4+} rings in a tetrahedral arrangement [29–31]. The 800 cm^{-1} band referred to vibrations of oxygen atoms in the boroxol ring with the participation of a very small movement of boron atoms [32,33]. The presence of broad bands in the high-frequency region (1250–1500 cm^{-1}) were associated with stretching of the $B–O^-$ terminal bonds in borate structures containing metaborate triangles [33–36].

We observed four additional bands: at 390, 650, 715, and 890 cm^{-1} for Bi-based glasses. The 390 cm^{-1} band was associated with the bending modes of the Ge–O–Ge [37]. The 650 cm^{-1} band was referred as vibrations of the 6-coordinated germanium atom in the glass structure [30,38]. The 890 cm^{-1} band is generally attributed with a double degenerate vibration [39]. According to the Ref. [31] the 715 cm^{-1} band characterized tensile vibrations of the B-sublattice relative to the O-sublattice and out-of-plane ring B–O–B vibration.

Table 2. Interpretation of Raman bands in Pb-based and Bi-based glasses.

Raman shift, cm^{-1}		Interpretation	Reference
Pb-based	**Bi-based**		
	390	Bending modes of Ge–O–Ge bonds	[37]
465	460	Symmetrical stretching of Ge–O–Ge bonds in 4- or 6-membered rings of Ge^{4+} in a tetrahedral arrangement	[29–31]
	650	Vibrations of 6-coordinated atom Ge (VI)	[30,38]
	715	Stretching vibration of the B-sublattice against the O-sublattice, a B–O–B out-of-plane ring vibration	[31]
800	800	Vibration of the oxygen atoms in the boroxol ring	[32,33]
	890	Ge–O–Ge double degenerate vibration	[39]
1315	1240	$B–O^-$ stretching mode in metaborate structures	[33–35]
1500		Overlap of following modes: $B–O^-$ in $BØ_2O^-$, $BØ_2O^-$ triangle linked to $BØ_4$ unit, and stretching in $BØ_3$ triangles	[36]

Preprints (www.preprints.org) | NOT PEER-REVIEWED | Posted: 4 January 2024 doi:10.20944/preprints202401.0267.v1

The Fourier transform infrared spectra were interpreted based on the assumption that the B–O and O–Ge–O bonds play a key role in the glass structure. The FT-IR spectra of bismuth/lead borogermanate glasses doped with Sm^{3+} and Gd^{3+} ions were investigated in the 500–2000 cm^{-1} range (Figure S4-S5). All analyzed glass samples demonstrated active vibrational modes, indicating the presence of typical characteristics for a borogermanate glass network.

The 540 and 544 cm^{-1} bands referred to the deforming vibrations of the Ge–O bond [40]. The 773 cm^{-1} band was related to the Ge–O stretching vibrations in the structural units [GeO_4] [40,41]. Bands in the mid-frequency region (>800 cm^{-1}) at 805, 1170, 1185, 1450, and 1547 cm^{-1} described the stretching of the B–O bond. The 805 cm^{-1} band is attributed with [BO_4] unit stretching [34,41], while the bands at 1170, 1185, 1450, 1547 cm^{-1} are responsible for [BO_3] unit stretching [41,42].

An analysis of IR spectra obtained by FT-IR and Raman spectroscopies did not reveal any contradictions. Hypotheses regarding the structure of glass presented earlier [29–42] were confirmed.

3.3. DSC characterisation and physical properties

To determine the maximum operating temperature for luminescent thermometry for the obtained glasses we measured the glass transition temperatures by the DSC technique (Table 3, Figures S6-S17). To the date as an upper limit for the maximum operating temperature for luminescent thermometry we chose the 673 K temperature which was ~100 K lower the glass transition temperatures for all glasses.

Table 3. Glass transition temperature (T_g) of synthesized glasses.

Sample ID	T_g (K)	Sample ID	T_g (K)
(12.75)Pb(1.5)Sm(0.75)Gd-42.5	768	**(12.75)Bi(1.5)Sm(0.75)Gd-42.5**	772
(12)Pb(1.875)Sm(1.125)Gd-42.5	778	**(12)Bi(1.875)Sm(1.125)Gd-42.5**	795
(11.25)Pb(2.25)Sm(1.5)Gd-42.5	806	**(11.25)Bi(2.25)Sm(1.5)Gd-42.5**	802
(17)Pb(2.0)Sm(1.0)Gd-40	782	**(17)Bi(2.0)Sm(1.0)Gd-40**	796
(16)Pb(2.5)Sm(1.5)Gd-40	797	**(16)Bi(2.5)Sm(1.5)Gd-40**	804
(15)Pb(3.0)Sm(2.0)Gd-40	824	**(15)Bi(3.0)Sm(2.0)Gd-40**	810

The density of the samples naturally increases with an increase in the content of heavy metal oxide and a decrease in the content of B_2O_3 and GeO_2 (Table 4). The densities of Bi-based samples were higher compared to Pb-based ones, which could be associated with a higher Bi molecular weight [12]. A similar trend we observed for the refractive index (Table 4). It should be noted that the change in the content of lead oxide by ±1 mol. % did not significantly affect the refractive index values.

Table 4. Density and refractive indices of synthesized glasses.

Sample ID	Density (g/cm^3)	Refractive index at 589 nm	Sample ID	Density (g/cm^3)	Refractive index at 589 nm
(12.75)Pb(1.5)Sm(0.75)Gd-42.5	4.060	1.68	**(12.75)Bi(1.5)Sm(0.75)Gd-42.5**	4.655	1.78
(12)Pb(1.875)Sm(1.125)Gd-42.5	4.030	1.68	**(12)Bi(1.875)Sm(1.125)Gd-42.5**	4.630	1.77
(11.25)Pb(2.25)Sm(1.5)Gd-42.5	4.015	1.68	**(11.25)Bi(2.25)Sm(1.5)Gd-42.5**	4.600	1.76
(17)Pb(2.0)Sm(1.0)Gd-40	4.390	1.72	**(17)Bi(2.0)Sm(1.0)Gd-40**	5.060	1.82
(16)Pb(2.5)Sm(1.5)Gd-40	4.370	1.72	**(16)Bi(2.5)Sm(1.5)Gd-40**	5.010	1.80
(15)Pb(3.0)Sm(2.0)Gd-40	4.270	1.72	**(15)Bi(3.0)Sm(2.0)Gd-40**	4.990	1.78

Preprints (www.preprints.org) | NOT PEER-REVIEWED | Posted: 4 January 2024 doi:10.20944/preprints202401.0267.v1

3.4. Spectral-luminescent properties

We observed that the absorption spectrum of Pb-based glasses (Figure 3) included 11 main bands associated with *f–f* transitions from the ground state ($^6H_{5/2}$) to various excited states of Sm^{3+}. The transition to the $^6P_{3/2}$ state at 402 nm is the most intense, since the 4*f* electrons are screened by the 5*s* and 5*p* shells [43]. The remaining absorption bands are observed in the IR region. The most intense band corresponds to the $^6H_{5/2} \rightarrow {}^6F_{7/2}$ transition. The intensity of all absorption bands increased with increasing content of Sm^{3+} in the obtained Pb-based glasses.

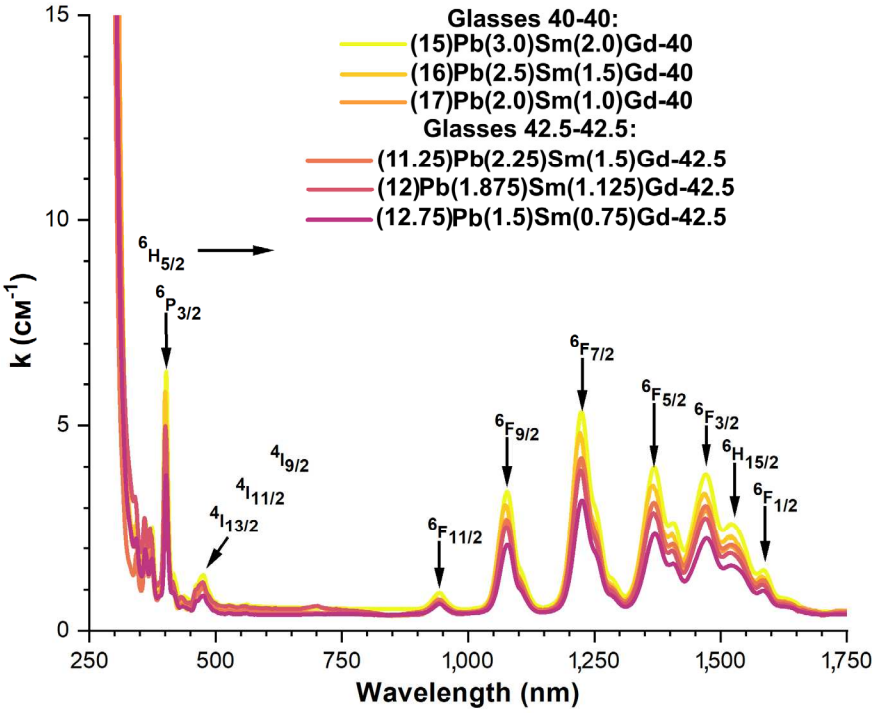

Figure 3. Optical absorption spectra of synthesized Pb-based glasses.

The absorption spectra of Bi-based samples similarly included the above 11 bands specific for Sm^{3+} (Figure 4). The bands attributed to the $^4I_{9/2}$, $^4I_{11/2}$ and $^4I_{13/2}$ transitions (~475 nm) are invisible, since the absorption in the region of 500 nm of bismuth active centers (BACs) overlaps these bands [28,45]. An increase in the Bi_2O_3 concentration resulted in the intensity growth of 475 nm band, and in a shift of the short-wavelength absorption edge to the long-wavelength region, which led to a narrowing of the transparency window of the Bi-based glasses.

Preprints (www.preprints.org) | NOT PEER-REVIEWED | Posted: 4 January 2024 doi:10.20944/preprints202401.0267.v1

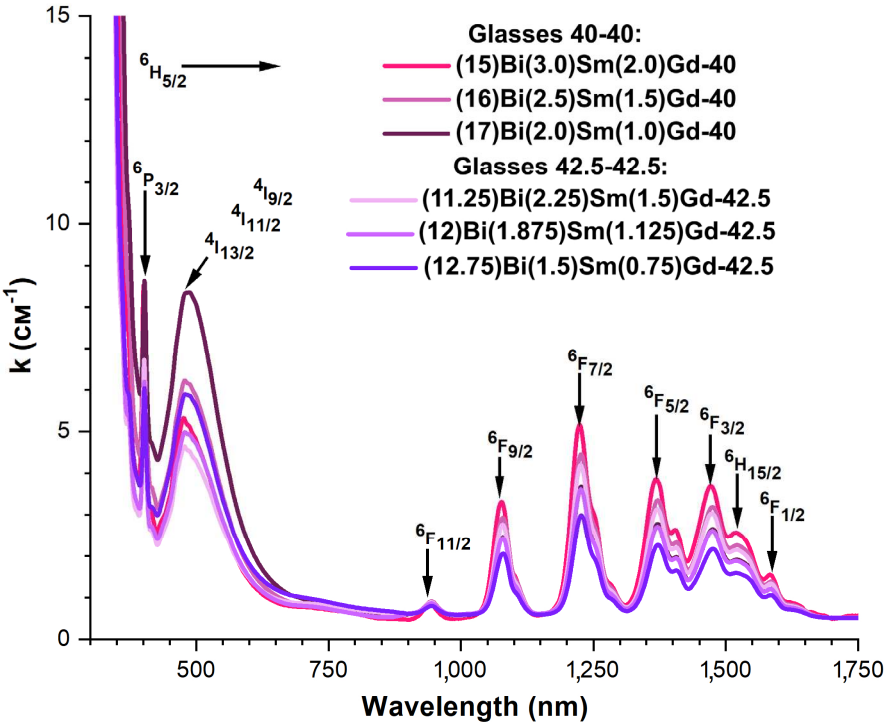

Figure 4. Optical absorption spectra of synthesized Bi-based glasses.

The intensive excitation band for all glasses was observed around 400 nm (Figure 5, S18). The intensity of the $^6H_{5/2} \rightarrow {}^4K_{11/2}$ transition at 404 nm is the highest regardless of the composition.

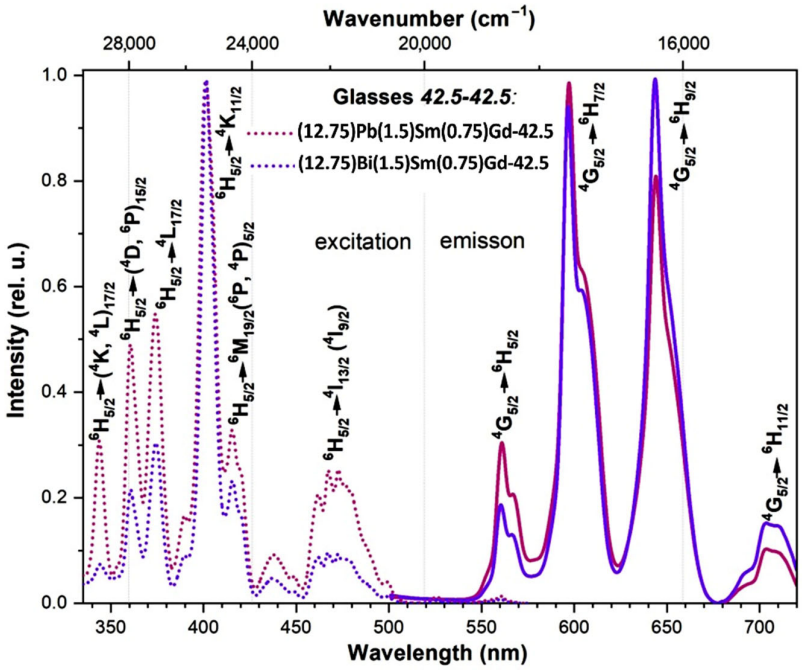

Figure 5. Emission (λ^{ex} = 377 nm) and excitation (λ^{em} = 595 nm) spectra of (12.75)Pb(1.5)Sm(0.75)Gd-42.5 and (12.75)Bi(1.5)Sm(0.75)Gd-42.5 glasses.

The photoluminescence (PL) spectra of glasses (Figure 6) revealed the Sm^{3+} bands at 562 nm ($^4G_{5/2} \rightarrow {}^6H_{5/2}$), 597 nm ($^4G_{5/2} \rightarrow {}^6H_{7/2}$), 645 nm ($^4G_{5/2} \rightarrow {}^6H_{9/2}$) and 704 nm ($^4G_{5/2} \rightarrow {}^6H_{11/2}$) resulted from the

Preprints (www.preprints.org) | NOT PEER-REVIEWED | Posted: 4 January 2024 doi:10.20944/preprints202401.0267.v1

transitions between 4*f*–4*f* levels. The most intense transition is $^4G_{5/2} \rightarrow {}^6H_{7/2}$, which corresponds to the orange luminescence. An increase in the Sm^{3+} ion concentration led to concentration quenching. In the obtained glasses Gd^{3+} played a role of a sensitizer with respect to Sm^{3+} [46]. The presence of Gd^{3+} increased the PL intensity in times. The most intense luminescence was obtained for the (12.75)Pb(1.5)Sm(0.75)Gd-42.5 and (12.75)Bi(1.5)Sm(0.75)Gd-42.5 glass samples.

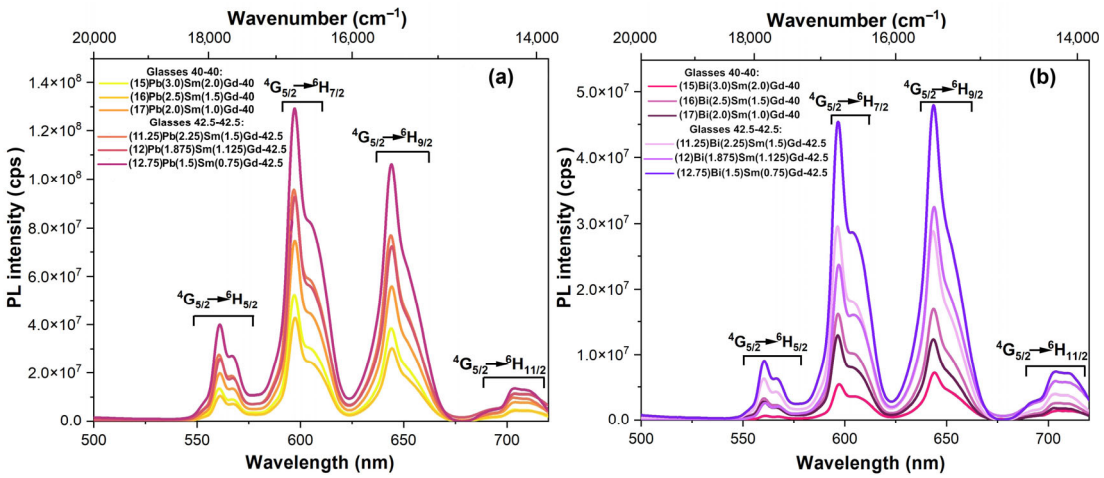

Figure 6. Emission spectra of Pb-based (a) and Bi-based (b) glass samples (λ^{ex}=404 nm).

An analysis of PL kinetics (Figure 7, for details see Figure S19-S30) showed that the decay curves could be described by bi-exponential decay kinetics. The fast PL centers had the lifetime of 90-100 ns while the slow PL centers had the lifetime of 590-620 ns (Table 5).

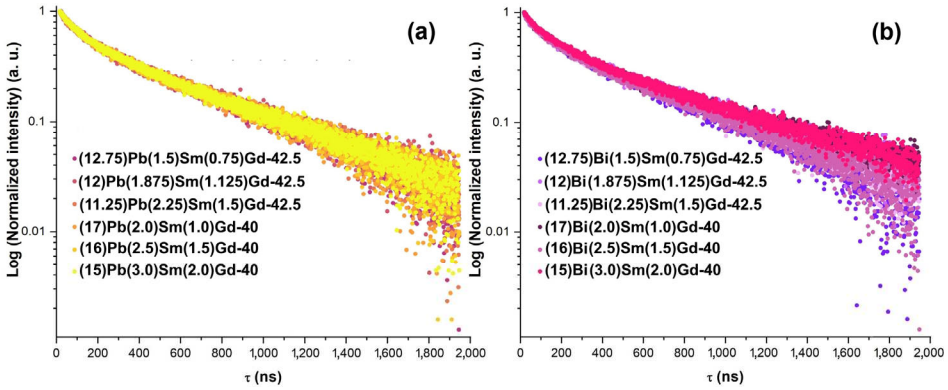

Figure 7. Time-resolved photoluminescence decay curve of Pb-based (a) and Bi-based (b) glass samples measured at λ^{PL}=597 nm.

Table 5. Pl decay kinetics parameters of samples generated from the curve fitting.

Sample ID	τ_1, (ns)	τ_2, (ns)	Sample ID	τ_1, (ns)	τ_2, (ns)
(12.75)Pb(1.5)Sm(0.75)Gd-42.5	95.3 ± 1.9	608.8 ± 7.9	**(12.75)Bi(1.5)Sm(0.75)Gd-42.5**	101.6 ± 2.2	609.0 ± 8.6
(12)Pb(1.875)Sm(1.125)Gd-42.5	98.7 ± 2.0	618.7 ± 8.7	**(12)Bi(1.875)Sm(1.125)Gd-42.5**	99.9 ± 2.1	619.7 ± 8.9
(11.25)Pb(2.25)Sm(1.5)Gd-42.5	97.9 ± 2.2	604.6 ± 8.8	**(11.25)Bi(2.25)Sm(1.5)Gd-42.5**	95.6 ± 1.9	586.0 ± 7.4
(17)Pb(2.0)Sm(1.0)Gd-40	100.4 ± 2.0	616.4 ± 8.5	**(17)Bi(2.0)Sm(1.0)Gd-40**	99.8 ± 2.1	617.7 ± 8.7
(16)Pb(2.5)Sm(1.5)Gd-40	93.4 ± 2.3	600.6 ± 8.8	**(16)Bi(2.5)Sm(1.5)Gd-40**	97.0 ± 2.2	623.4 ± 9.4
(15)Pb(3.0)Sm(2.0)Gd-40	96.9 ± 2.3	604.5 ± 7.9	**(15)Bi(3.0)Sm(2.0)Gd-40**	96.9 ± 2.1	602.7 ± 8.3

Preprints (www.preprints.org) | NOT PEER-REVIEWED | Posted: 4 January 2024 doi:10.20944/preprints202401.0267.v1

The (12.75)Pb(1.5)Sm(0.75)Gd-42.5 and (12.75)Bi(1.5)Sm(0.75)Gd-42.5 glass samples demonstrated the most intensive PL (Figure 7, 8) and they were chosen for the testing of LT properties in the 298–673 K temperature range.

At temperature rise, the (12.75)Pb(1.5)Sm(0.75)Gd-42.5 sample demonstrated an appearance of 525–542 nm band starting with 423 K and its further growth up to 673 K, which could be associated with an increase in the population of the overlying $^4F_{3/2}$ state due to transitions from the $^4G_{5/2}$ level in samarium ions under the influence of temperature [47]. Simultaneously, the most intensive 597 and 645 nm bands gradually reduced at temperature rise from 423 to 673 K in 1.4 times maximum (Figure 8).

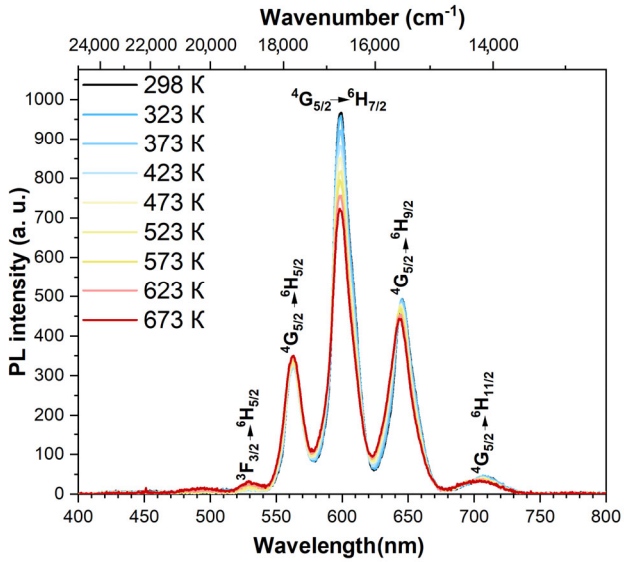

Figure 8. Emission spectra of $Pb_{12.75}Sm_{1.5}Gd_{0.75}$ recorded at different temperatures (λ^{ex} = 404 nm).

It is of common use that FIR is calculated using the ratio of normalized intensities of the band (Figure 9a). So, calculate FIR in the 423 to 673 K temperature range we used PL intensity of the $^4F_{3/2} \rightarrow {}^6H_{5/2}$ transition (λ_{PL}^{max} = 530 nm) as a constant value of numerator while for a denominator the PL intensities of the $^4G_{5/2} \rightarrow {}^6H_{5/2}$ (λ_{PL}^{max} = 562 nm); $^4G_{5/2} \rightarrow {}^6H_{7/2}$ (λ_{PL}^{max} = 597 nm); $^4G_{5/2} \rightarrow {}^6H_{9/2}$ (λ_{PL}^{max} = 645 nm) transitions were used (Figure 9b). At temperature increase starting from 423 K the PL peak at 535 nm attributed with $^4F_{3/2} \rightarrow {}^6H_{5/2}$ transition has been growing up. Using this thermosensitive transition for the numerator and thermostable transition $^4G_{5/2} \rightarrow {}^6H_{7/2}$ as the denominator we calculated FIR according to the equation (7).

$$FIR = \frac{I_{^4F_{3/2} \rightarrow {}^6H_{5/2}}}{I_{^4G_{5/2} \rightarrow {}^6H_{7/2}}}, \quad (7)$$

Preprints (www.preprints.org) | NOT PEER-REVIEWED | Posted: 4 January 2024 doi:10.20944/preprints202401.0267.v1

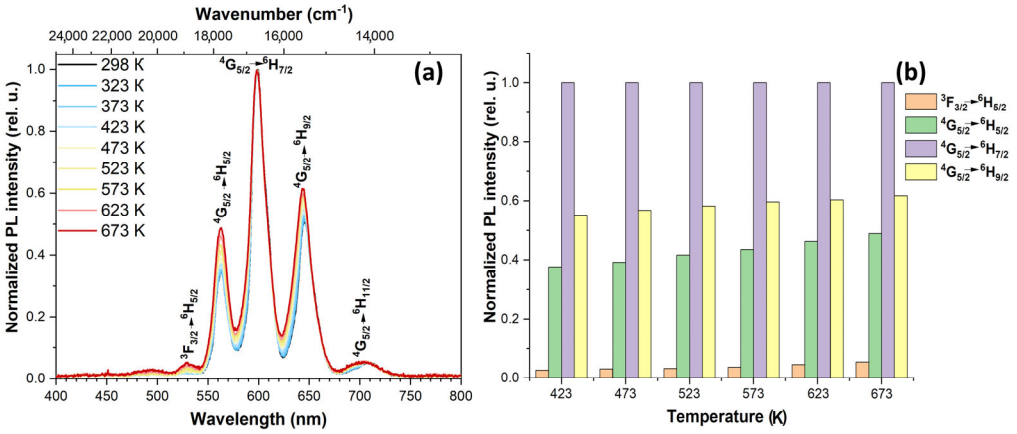

Figure 9. Normalized emission spectra (a) of (12.75)Pb(1.5)Sm(0.75)Gd-42.5 glass sample recorded at different temperatures (λ^{ex} = 404 nm) and normalized PL intensities of the bands (b), corresponding to the transitions in Sm^{3+}.

The temperature dependence of FIR was approximated by a linear function (FIR = $a + b \times T$) (Figure 10a) and an exponential Boltzmann function (FIR= $a \times exp^{-\Delta E/kT} + b$) (Figure 10b). Regardless of the function the best descriptions of the obtained experimental data of FIR was calculated for the transitions I($^4F_{3/2} \rightarrow {}^6H_{5/2}$)/I($^4G_{5/2} \rightarrow {}^6H_{7/2}$) FIR=$I_{535}/I_{645}$. We obtained Adj. R^2=0.90644 for linear function and Adj. R^2=0.97815 for the Boltzmann function.

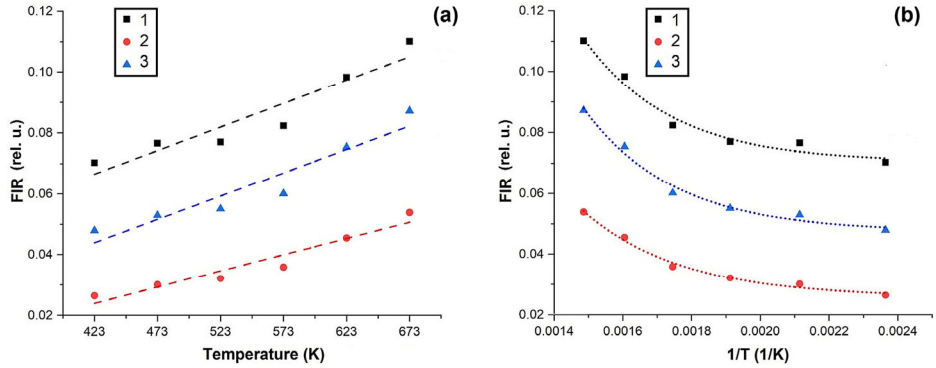

Figure 10. The temperature dependence of the ratio of luminescence intensities between the transitions for (12.75)Pb(1.5)Sm(0.75)Gd-42.5 sample described by linear (**a**) and Boltzmann equations (**b**): (**1**) - I($^4F_{3/2} \rightarrow {}^6H_{5/2}$)/I($^4G_{5/2} \rightarrow {}^6H_{5/2}$); (**2**) - I($^4F_{3/2} \rightarrow {}^6H_{5/2}$)/I($^4G_{5/2} \rightarrow {}^6H_{7/2}$); (**3**) - I($^4F_{3/2} \rightarrow {}^6H_{5/2}$)/I($^4G_{5/2} \rightarrow {}^6H_{9/2}$).

The relative thermal sensitivity (S_r) for the parameter under consideration was obtained S_r ~0.20 %×K^{-1} for the temperature range 423–673 K.

We tried to increase FIR sensitivity by manipulation of different peak intensities. Indeed, when calculating FIR as a ratio

$$FIR = Q = \frac{I_1}{I_2}, \quad (8)$$

to increase the sensitivity S_r we need to reduce the denominator at temperature growth.

In the case of (12.75)Pb(1.5)Sm(0.75)Gd-42.5 sample the generalized picture of relative PL intensities redistribution with temperature are presented in Figure 11b. The PL intensity of $^4F_{3/2} \rightarrow {}^6H_{5/2}$ transition is growing up in 2 times. And this resulted to increase of the nominator in Eq. 7. But the denominator associated with PL intensity of $^4G_{5/2} \rightarrow {}^6H_{7/2}$ transition stayed unchangeable. We need to reduce the denominator. To do this we can use the difference of the constant PL intensity of $^4G_{5/2}$

Preprints (www.preprints.org) | NOT PEER-REVIEWED | Posted: 4 January 2024 doi:10.20944/preprints202401.0267.v1

→ $^6H_{7/2}$ transition and growing up PL intensity of $^4G_{5/2} \rightarrow {}^6H_{9/2}$ or $^4G_{5/2} \rightarrow {}^6H_{5/2}$. Both of the latters are temperature sensitive transitions. In this case new efficient FIR_{eff} could be calculated from the expression

$$FIR_{eff}(1) = \frac{I_{^4F_{3/2}\rightarrow {}^6H_{5/2}}}{I_{^4G_{5/2}\rightarrow {}^6H_{7/2}} - I_{^4G_{5/2}\rightarrow {}^6H_{5/2}}}, \quad (9)$$

$$FIR_{eff}(2) = \frac{I_{^4F_{3/2}\rightarrow {}^6H_{5/2}}}{I_{^4G_{5/2}\rightarrow {}^6H_{7/2}} - I_{^4G_{5/2}\rightarrow {}^6H_{9/2}}}, \quad (10)$$

Figure 11 demonstrated the privilege of such approach when using the same raw data one can increase S_r in several times by manipulations of the PL intensities from different T-sensitive and non-sensitive transitions.

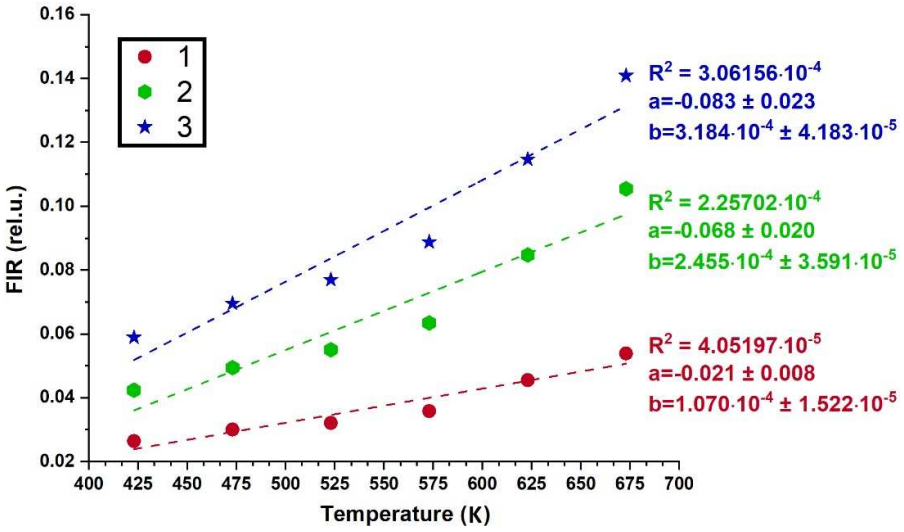

Figure 11. The temperature dependence of FIR for (12.75)Pb(1.5)Sm(0.75)Gd-42.5 sample calculated using the Eq.(7) red dots (1); Eq.(9) green dots (2), Eq.(10) blue dots (3).

For the (12.75)Pb(1.5)Sm(0.75)Gd-42.5 sample the corresponding sensitivities for different FIRs occurred to be $S_r(1)$ = 0.20 %×K^{-1}; $S_r(2)$ = 0.68 %×K^{-1}; $S_r(3)$ = 0.61 %×K^{-1}. The better achieved sensitivity was more than in 3 times higher than that determined by the classical expression (7).

In the series of Bi-based samples, the most interesting was the (17)Bi(2)Sm(1)Gd-40 glass. We detected a redistribution of the intensities of the peaks corresponding to the $^4G_{5/2} \rightarrow {}^6H_{7/2}$ and $^4G_{5/2} \rightarrow {}^6H_{9/2}$ transitions (Figure 12, 13a). This redistribution is a temperature-sensitive parameter, which could be used for temperature determination. Such redistribution is usually observed for dyes [48], but we found out it for the glass sample for the first time.

Preprints (www.preprints.org) | NOT PEER-REVIEWED | Posted: 4 January 2024 doi:10.20944/preprints202401.0267.v1

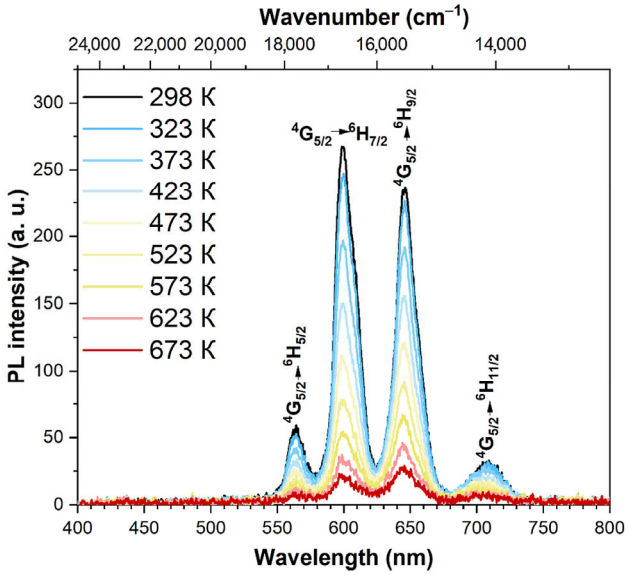

Figure 12. Emission spectra of (17)Bi(2)Sm(1)Gd-40 glass recorded at different temperatures (λ^{ex} = 404 nm).

So, calculating FIR in 298–673 K temperature range we tried to choose the most sensitive parameter based on PL intensities of the bands which had been redistributed: $^4G_{5/2} \rightarrow {}^6H_{9/2}$ (λ_{PL}^{max} = 645 nm) or $^4G_{5/2} \rightarrow {}^6H_{7/2}$ (λ_{PL}^{max} = 597 nm) (Figure 13b).

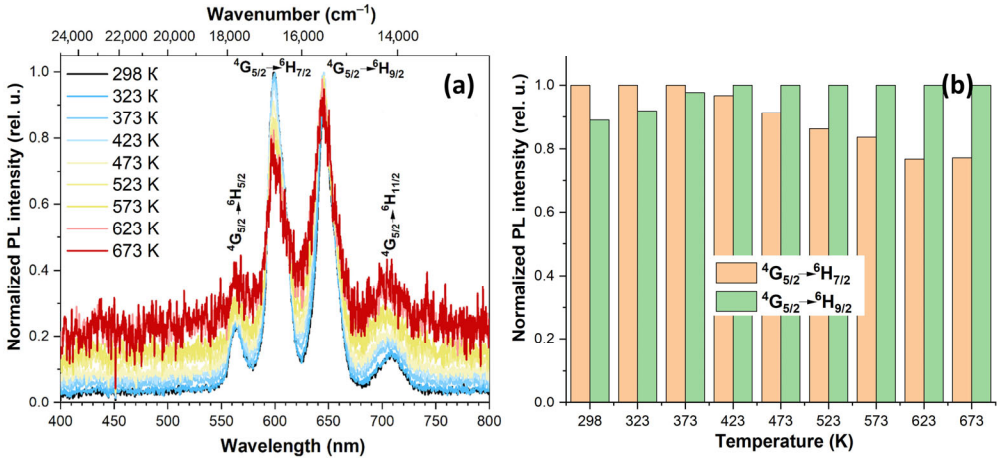

Figure 13. Normalized emission spectra (a) of (17)Bi(2)Sm(1)Gd-40 glass sample recorded at different temperatures (λ^{ex} = 404 nm) and normalized PL intensities of the bands (b), corresponding to the transitions in Sm^{3+}.

We varied the PL intensities ratio by changing nominator and denominator vice versa. The better approximation was derived for linear function when the I($^4G_{5/2} \rightarrow {}^6H_{7/2}$)/I($^4G_{5/2} \rightarrow {}^6H_{9/2}$) ratio was used (Figure 14a). Contrary, for the Boltzmann function the better result was achieved for the I($^4G_{5/2} \rightarrow {}^6H_{9/2}$)/I($^4G_{5/2} \rightarrow {}^6H_{7/2}$) ratio (Figure 14b). But taking into consideration the accuracy of the experimental data both these functions could be used in the case of (17)Bi(2)Sm(1)Gd-40 glass for luminescent thermometry. The relative thermal sensitivity for the considered parameter was ~0.105 %×K^{-1} for 298-673 K temperature range.

Preprints (www.preprints.org) | NOT PEER-REVIEWED | Posted: 4 January 2024 doi:10.20944/preprints202401.0267.v1

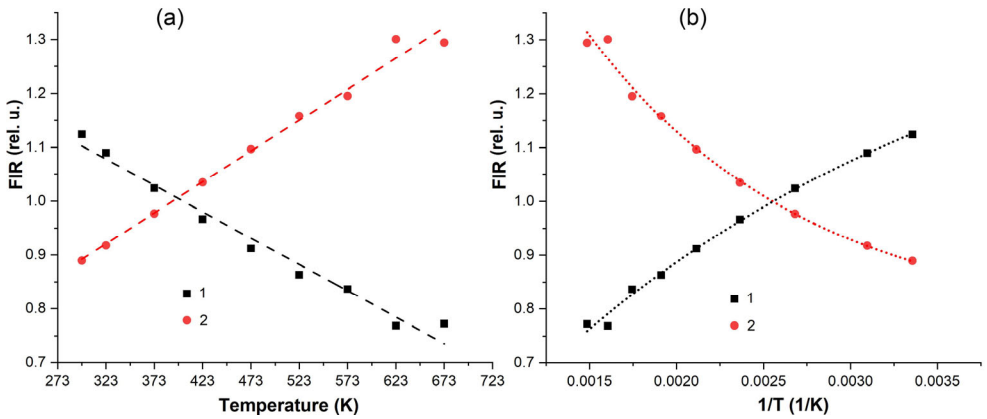

Figure 14. The temperature dependence of the ratio of luminescence intensities between the transitions for $Pb_{12.75}Sm_{1.5}Gd_{0.75}$ sample described by linear (**a**) and Boltzmann equations (**b**): (**1**) - $I(^4G_{5/2} \rightarrow {}^6H_{9/2})/I(^4G_{5/2} \rightarrow {}^6H_{7/2})$; (**2**) - $I(^4G_{5/2} \rightarrow {}^6H_{7/2})/I(^4G_{5/2} \rightarrow {}^6H_{9/2})$.

4. Discussion

Decay kinetics studies let us better understand the nature of PL mechanism in the analyzed samples. The obtained values of life-time in our research are in order smaller than those described in Ref. [46,49–52]. And in the majority of publications the authors presented one-exponential decay kinetics when measured the millisecond range [48–50]. The transition to microsecond range resulted to detecting two-exponential kinetics [46,52]. In our experiments we investigated the nanosecond decay range, in which we found out two-exponential kinetics with the contribution of the fast component was ~40%.

Decay kinetics studies demonstrate that the addition of Gd^{3+} ions provides an additional energy transfer mechanism, resulting in a decay time increase. Initially, the absorbed energy is transferred from the matrix to Gd^{3+} ions, and then further to the Sm^{3+} ions, which results to two different luminescent centers and affects the total decay time. This mechanism was also discussed in Ref. [46] and the authors came to the same conclusions.

In Pb-based glasses there is no specific dependence on the decay time, which correlates with the absence of absorption bands in 500-600 nm region (Figure 3). While in Bi-based glasses, an increase in the matrix content reduces the short life-time value, since the BACs additionally interacts with Sm^{3+} ions and in 500-600 nm region, the Bi-contained matrix has a characteristic absorption band (Figure 4).

In previous studies [43] devoted to the use of similar glasses as materials for non-contact thermometers, a relatively narrow operating temperature range (288-333 K) was considered with S_r = 1.68%×K^{-1} (288 K) and S_r = 1.25 %×K^{-1} (333 K). We have expanded the working range to 298-673 K and found out that Pb-based glasses could give S_r = 0.68%×K^{-1} (423-673 K) while Bi-based glasses had rather low S_r = 0.105%×K^{-1}. So, we could not replace the toxic Pb-based glasses on non-toxic Bi-based glasses in LT applications for the large temperature range.

In the case of Bi-based glass one of the problem for LT is the interference of BACs with PL band if RE^{3+} ions. To solve the problem one can suppress BACs by introducing of alkali ions in a large amount [37]. But the LT properties of such glasses need the further investigation.

The achieved values of S_r in a wide temperature range open up real prospects for the use of the Pb-based glasses for thermal detection in medicine, energy and industry. In addition, in contrast to the previous study [43], we recorded not only changes in the PL peak intensity, but also in the redistribution of intensities between peaks, as well as the appearance of new peaks for the temperature measurement. Using the multiply function for FIR, which taking into account both thermal sensitive and non-sensitive transitions we have succeeded to increase the sensitivity of LT materials in 3.4 times.

 doi:10.20944/preprints202401.0267.v1

It is worth emphasizing that the borogermanate matrix, thanks to GeO_2, is characterized by low phonon energy, while the presence of B_2O_3 enhances the glass's resistance to thermal influences, which is critical for thermoluminescence detector operating in a wide temperature range.

5. Conclusions

Sm^{3+}/Gd^{3+} co-doped glasses in the B_2O_3–GeO_2–PbO and B_2O_3–GeO_2–Bi_2O_3 systems were fabricated by conventional glass technology. The structural, optical and luminescence properties of the glasses have been studied. It was demonstrated that the obtained glasses revealed the photoluminescence in the wide temperature range of 298-673 K. The best temperature-sensitive luminescence was found out for (12.75)Pb(1.5)Sm(0.75)Gd-42.5 and (17)Bi(2)Sm(1)Gd-40 glass samples. An increase in temperature led to an increase in the population of the $^4F_{3/2}$ Sm^{3+} state due to transitions from the lower $^4S_{3/2}$ level for glasses under study.

The thermal sensitivity for the (12.75)Pb(1.5)Sm(0.75)Gd-42.5 glass sample was estimated to be about 0.250 %×K^{-1} and for the (17)Bi(2)Sm(1)Gd-40 glass sample ~0.105 %×K^{-1} based on the ratio of the luminescence intensities of transitions from different Stark sublevels.

For the first time we found out the effect of Bi-based samples, the most interesting was. We detected a redistribution of the intensities of the peaks corresponding to the $^4G_{5/2} \rightarrow {}^6H_{7/2}$ and $^4G_{5/2} \rightarrow {}^6H_{9/2}$ transitions in the inorganic phosphor (17)Bi(2)Sm(1)Gd-40 glass which is usually observed for dyes.

We used two temperature sensitive and one non-sensitive transitions to calculate FIR. This made it possible to increase the sensitivity of LT in several times. Such method could be very useful for the LT materials based on Ln ions with multiplied transitions.

The results showed that the produced glasses are perspective for photonics applications, in particular in luminescence thermometry.

Supplementary Materials: The following supporting information can be downloaded at: www.mdpi.com/xxx/s1, Figure S1. PXRD patterns of Pb-based (a) and Bi-based (b) glass samples; Figure S2. Raman spectra of Pb-based glass samples; Figure S3. Raman spectra of Bi-based glass samples; Figure S4. FT-IR spectra of Pb-based glass samples; Figure S5. FT-IR spectra of Bi-based glass samples; Figure S6. DSC curve for glass composition (15)Pb(3)Sm(2)Gd-40 and glass transition temperature; Figure S7. DSC curve for glass composition (16)Pb(2.5)Sm(1.5)Gd-40 and glass transition temperature; Figure S8. DSC curve for glass composition (17)Pb(2)Sm(1)Gd-40 and glass transition temperature; Figure S9. DSC curve for glass composition (11.25)Pb(2.25)Sm(1.5)Gd-42.5 and glass transition temperature; Figure S10 DSC curve for glass composition (12)Pb(1.875)Sm(1.125)Gd-42.5 and glass transition temperature; Figure S11. DSC curve for glass composition (12.75)Pb(1.5)Sm(0.75)Gd-42.5 and glass transition temperature; Figure S12. DSC curve for glass composition (15)Bi(3)Sm(2)Gd-40 and glass transition temperature; Figure S13. DSC curve for glass composition (16)Bi(2.5)Sm(1.5)Gd-40 and glass transition temperature; Figure S14. DSC curve for glass composition (17)Bi(2)Sm(1)Gd-40 and glass transition temperature; Figure S15. DSC curve for glass composition (11.25)Bi(2.25)Sm(1.5)Gd-42.5 and glass transition temperature; Figure S16. DSC curve for glass composition (12)Bi(1.875)Sm(1.125)Gd-42.5 and glass transition temperature; Figure S17. DSC curve for glass composition (12.75)Bi(1.5)Sm(0.75)Gd-42.5 and glass transition temperature; Figure S18. Excitation (λ^{em} = 595 nm) spectra of (15-17)Pb/Bi(3-2)Sm(2-1)Gd-40 and (11.25-12.75)Pb/Bi(2.25-1.5)Sm(1.5-0.75)Gd-42.5 glasses; Figure S19. Time resolved PL decay curve of (15)Pb(3)Sm(2)Gd-40 glass (λ^{PL} = 597 nm); Figure S20 Time resolved PL decay curve of (16)Pb(2.5)Sm(1.5)Gd-40 (λ^{PL} = 597 nm); Figure S21. Time resolved PL decay curve of (17)Pb(2)Sm(1)Gd-40 glass (λ^{PL} = 597 nm); Figure S22. Time resolved PL decay curve of (11.25)Pb(2.25)Sm(1.5)Gd-42.5 glass (λ^{PL} = 597 nm); Figure S23. Time resolved PL decay curve of (12)Pb(1.875)Sm(1.125)Gd-42.5 glass (λ^{PL} = 597 nm); Figure S24. Time resolved PL decay curve of (12.75)Pb(1.5)Sm(0.75)Gd-42.5 glass (λ^{PL} = 597 nm); Figure S25. Time resolved PL decay curve of (15)Bi(3)Sm(2)Gd-40 (λ^{PL} = 597 nm); Figure S26. Time resolved PL decay curve of (16)Bi(2.5)Sm(1.5)Gd-40 glass (λ^{PL} = 597 nm); Figure S27. Time resolved PL decay curve of (17)Bi(2)Sm(1)Gd-40 glass (λ^{PL} = 597 nm); Figure S28. Time resolved PL decay curve of (11.25)Bi(2.25)Sm(1.5)Gd-42.5 glass (λ^{PL} = 597 nm); Figure S29. Time resolved PL decay curve of (12)Bi(1.875)Sm(1.125)Gd-42.5 glass (λ^{PL} = 597 nm); Figure S30. Time resolved PL decay curve of (12.75)Bi(1.5)Sm(0.75)Gd-42.5 glass (λ^{PL} = 597 nm); Figure S31. EDS spectra of (15)Pb(3)Sm(2)Gd-40 glass composition; Figure S32. EDS spectra of (16)Pb(2.5)Sm(1.5)Gd-40 glass composition; Figure S33. EDS spectra of (17)Pb(2)Sm(1)Gd-40 glass composition; Figure S34. EDS spectra of (11.25)Pb(2.25)Sm(1.5)Gd-42.5 glass composition; Figure S35. EDS spectra of (12)Pb(1.875)Sm(1.125)Gd-42.5 glass composition; Figure S36. EDS spectra of (12.75)Pb(1.5)Sm(0.75)Gd-42.5 glass composition; Figure S37. EDS spectra of (15)Bi(3)Sm(2)Gd-40 glass composition; Figure S38. EDS spectra of (16)Bi(2.5)Sm(1.5)Gd-40 glass

composition; Figure S39. EDS spectra of (17)Bi(2)Sm(1)Gd-40 glass composition; Figure S40. EDS spectra of (11.25)Bi(2.25)Sm(1.5)Gd-42.5 glass composition; Figure S41. EDS spectra of (12)Bi(1.875)Sm(1.125)Gd-42.5 glass composition; Figure S42. EDS spectra of (12.75)Pb(1.5)Sm(0.75)Gd-42.5 glass composition; Table S1. The composition of glasses according to the EDS data collected from 10 points distributed randomly on the surface of the every samples.

Author Contributions: Conceptualization, O.P., S.Z. and K.S.; methodology, S.Z. and K.S.; software, K.B.; validation, S.Z. and K.S.; formal analysis, I.A.; investigation, S.Z., K.S., K.R., K.B.; resources, K.R.; data curation, K.R.; writing—original draft preparation, S.Z. and K.S.; writing—review and editing, S.Z.; visualization, S.Z. and K.S.; supervision, K.R.; project administration, I.A.; funding acquisition, K.R. All authors have read and agreed to the published version of the manuscript.

Funding: This research was funded by the Ministry of Science and Higher Education of Russia through the project FSSM-2020-0005.

Institutional Review Board Statement: Not applicable.

Informed Consent Statement: Not applicable.

Data Availability Statement: Not applicable.

Acknowledgments: The authors are grateful to the Mendeleev Center for the Collective Use of Scientific Equipment for the optical measurements.

Conflicts of Interest: The authors declare no conflict of interest.

References

1. Childs, P. R. N.; Greenwood, J. R.; Long, C. A. Review of temperature measurement. *Rev. Sci. Instrum.* **2000**, *71*, 2959–2978. https://doi.org/10.1063/1.1305516.
2. Michalski, L.; Eckersdorf, K.; Kucharski, J.; McGhee, J. *Temperature measurement.*; Publisher: Wiley, Chichester, UK, **2001**.
3. Beheim, G. Optical Temperature Sensors. Integrated Optics, Microstructures, and Sensors. 1995, 332, 285–313. https://doi.org/10.1007/978-1-4615-2273-7_12.
4. Wang, X.; Wolfbeis, O.S.; Meier, R. J. Luminescent probes and sensors for temperature. *Chem. Soc. Rev.* **2013**, *42, 19*, 7834–7869. https://doi.org/10.1039/C3CS60102A.
5. Brites, C.D.; Lima, P.P.; Silva, N.J.; Millán, A.; Amaral, V.S.; Palacio, F.; Carlos, L.D. A luminescent molecular thermometer for long-term absolute temperature measurements at the nanoscale. *Adv. Mater.* **2010**, *22, 40*, 4499–4504. https://doi.org/10.1002/adma.201001780.
6. Dramićanin, M.D. Trends in luminescence thermometry. *J. Appl. Phys.* **2020**, *128*, 4. https://doi.org/10.1063/5.0014825.
7. Sutton, G.; Korniliou, S.; Andreu, A.; Wilson, D. Imaging luminescence thermometry to 750 °C for the heat treatment of common engineering alloys and com-parison with thermal imaging. *Int. J. Thermophys.* **2022**, *43, 3*, 36. https://doi.org/10.1007/s10765-021-02963-1.
8. van Swieten, T.P.; Yu, D.; Yu, T.; Vonk, S.J.; Suta, M.; Zhang, Q.A.; Meijerink, A.; Rabouw, F.T. Ho^{3+}-based luminescent thermometer for sensitive sensing over a wide temperature range. *Adv. Opt. Mater*. **2021**, *9, 1*, 2001518. https://doi.org/10.1002/adom.202001518.
9. Bednarkiewicz, A.; Marciniak, L.; Carlos, L.D.; Jaque, D. Standardizing luminescence nanothermometry for biomedical applications. *Nanoscale*. **2020**, *12, 27*, 14405–14421.
10. Lan, C. W.; Yu, W. C.; Hsu, W. C. Growth of Bulk Single Crystals. In *Encyclopedia of Surface and Colloid Science, Third Edition*; CRC Press, 2016; pp 2979–2990. https://doi.org/10.1081/E-ESCS3-120039601.
11. Avetissov, I.; Kostikov, V.; Meshkov, V.; Sukhanova, E.; Grishechkin, M.; Belov, S.; Sadovskiy, A. Modeling of Axial Vibrational Control Technique for CdTe VGF Crystal Growth under Controlled Cadmium Partial Pressure. *J. Cryst. Growth* **2014**, *385*, 88–94. https://doi.org/10.1016/j.jcrysgro.2013.04.064.
12. Jaque, D.; Vetrone, F. Luminescence nanothermometry. *Nanoscale.* **2012**, *4, 15*, 4301–4326. https://doi.org/10.1039/C2NR30764B.
13. Abram, C.; Fond, B.; Beyrau, F. Temperature measurement techniques for gas and liquid flows using thermographic phosphor tracer particles. *Prog. Energy Combust. Sci.* **2018**, *64*, 93–156. https://doi.org/10.1016/j.pecs.2017.09.001.
14. Suta, M.; Antić, Ž.; Đorđević, V.; Kuzman, S.; Dramićanin, M.D.; Meijerink, A. Making Nd^{3+} a sensitive luminescent thermometer for physiological temperatures—An account of pitfalls in Boltzmann thermometry. *Nanomaterials*. **2020**, *10, 3*, 543. https://doi.org/10.3390/nano10030543.
15. Suo, H.; Zhao, X.; Zhang, Z.; Wang, Y.; Sun, J.; Jin, M.; Guo, C. Rational design of ratiometric luminescence thermometry based on thermally coupled levels for bioapplications. *Laser Photonics Rev.* **2021**, *15, 1*, 2000319. https://doi.org/10.1002/lpor.202000319.

16. Brities, C.D.S.; Millan, A. *Handbook on the Physics and Chemistry of Rare Earths*.; Publisher: Elsevier, North-Holland, **2016**, pp. 339–427.
17. Jaque, D.; Ramirez, M. O.; Bausá, L. E.; Solé, J. G.; Cavalli, E.; Speghini, A.; Bettinelli, M. $Nd^{3+} \rightarrow Yb^{3+}$ energy transfer in $YAl_3(BO_3)_4$ nonlinear laser crystal. *Phys. Rev. B.* **2003**, *68*, 35118. https://doi.org/10.1103/PhysRevB.68.035118.
18. Liu, X.; Akerboom, S.; de Jong, M.; Mutikainen, I.; Tanase, S.; Meijerink, A.; Bouwman, E. Mixed-Lanthanoid Metal–Organic Framework for Ratiometric Cryogenic Temperature Sensing. *Inorg. Chem.* **2015**, *54*, 11323-11329. https://doi.org/10.1021/acs.inorgchem.5b01924.
19. Brites, C. D. S.; Fiaczyk, K.; Ramalho, J. F. C. B.; Sójka, M.; Carlos, L. D.; Zych, E. Widening the Temperature Range of Luminescent Thermometers through the Intra- and Interconfigurational Transitions of Pr^{3+}. *Adv. Opt. Mater*. **2018**, *6*, 1701318. http://dx.doi.org/10.1002/adom.201701318.
20. Runowski, M.; Woźny, P.; Stopikowska, N.; Martin, I. R.; Lavin, V.; Lis, S. Luminescent Nanothermometer Operating at Very High Temperature—Sensing up to 1000 K with Upconverting Nanoparticles (Yb^{3+}/Tm^{3+}). *ACS Appl. Mater. Interfaces.* **2020**, *12*, 43933-43941. myyux244itm3twl46536576 4fhxfr m5h68566.
21. Allison, S. W.; Beshears, D. L.; Cates, M. R.; Scudiere, M. B.; Shaw, D. W.; Ellis, A. D. Luminescence of YAG:Dy and YAG:Dy, Er crystals to 1700 °C. *Meas. Sci. Technol.* **2019**, *31*, 044001. https://doi.org/10.1088/1361-6501/ab4ebd.
22. Herrera, A.; Buchner, S.; Camerini, R. V.; Jacinto, C.; Balzaretti, N. M. Spectroscopic properties of B_2O_3–PbO–Bi_2O_3–GeO_2 glass doped with Sm^{3+} and gold nanoparticles. *Opt. Mater.* **2016**, *52*, 230-236. https://doi.org/10.1016/j.optmat.2015.12.048.
23. Gökçe, M.; Koçyiğit, D. Structural and optical properties of Gd^{+3} doped Bi_2O_3–GeO_2 glasses and glass-ceramics. *Mater. Res. Express*. **2018**, *6*, *2*, 025203. https://doi.org/10.1088/2053-1591/aaee53.
24. Gökçe, M.; Koçyiğit, D. Optical and luminescence characteristics of Sm^{3+} doped B_2O_3-GeO_2-Gd_2O_3 glasses. *Opt. Mater.* **2018**, *83*, 233-240. https://doi.org/10.1016/j.optmat.2018.06.015.
25. Lakshminarayana, G.; Meza-Rocha, A. N.; Soriano-Romero, O.; Huerta, E. F.; Caldino, U.; Lira, A.; Lee, D.-E.; Yoon, J.; Park, T. Analysis of fluorescence characteristics of Sm^{3+}-doped B_2O_3-rich glasses for Orange-light-emitting diodes. *J. Alloys Compd.* **2021**, *884*, 161076. https://doi.org/10.1016/j.jallcom.2021.161076.
26. Herrera, A.; Fernandes, R. G.; de Camargo, A. S. S.; Hernandes, A. C.; Buchnerd, S.; Jacinto, C.; Balzaretti, N. M. Visible-NIR emission and structural properties of Sm^{3+} doped heavy-metal oxide glass with composition B_2O_3-PbO-Bi_2O_3-GeO_2. *J. Lumin.* **2015**, *171*, 106-111. http://dx.doi.org/10.1016/j.jlumin.2015.10.065.
27. Rammah, Y.S.; Mahmoud, K.A.; Kavaz, E.; Kumar, A.; El-Agawany, F.I. The role of PbO/Bi_2O_3 insertion on the shielding characteristics of novel borate glasses. *Ceram. Int.* **2020**, *46*, *15*, 23357–23368. https://doi.org/10.1016/j.ceramint.2020.04.018.
28. Denker, B.; Galagan, B.; Osiko, V.; Sverchkov, S.; Dianov, E. Luminescent properties of Bi-doped boro-alumino-phosphate glasses. *J. Appl. Phys.* **2007**, *87*, 135–137. https://doi.org/10.1007/s00340-006-2518-1.
29. Ren, J.; Eckert, H. Quantification of Short and Medium Range Order in Mixed Network Former Glasses of the System GeO_2–$NaPO_3$: A Combined NMR and X-Ray Photoelectron Spectroscopy Study. *J. Phys. Chem. C*. **2012**, *116*, *23*, 12747−12763. https://doi.org/10.1021/jp301383x.
30. Di Martino, D.; Santos, L.F.; Marques, A.C.; Almeida, R.M. Vibrational Spectra and Structure of Alkali Germanate Glasses. *J. Non-Cryst. Solids*. **2001**, *293*, 394−401. https://doi.org/10.1016/S0022-3093(01)00690-1.
31. Chakraborty, I.N.; Condrate, R.A. The Vibrational Spectra of B_2O_3-GeO_2 Glasses. *J. Non-Cryst. Solids*. **1986**, *81*, *3*, 271−284. https://doi.org/10.1016/0022-3093(86)90496-5.
32. Meera, B. N.; Sood, A. K.; Chandrabhas, N.; Ramakrishna, J. Raman study of lead borate glasses. *J. Non-Cryst. Solids*. **1990**, *126*, *3*, 224–230. https://doi.org/10.1016/0022-3093(90)90823-5.
33. Yano, T.; Kunimine, N.; Shibata, S.; Yamane, M. Structural Investigation of Sodium Borate Glasses and Melts by Raman Spectroscopy. II. Conversion between BO_4 and BO_2O^- Units at High Temperature. *J. Non-Cryst. Solids*. **2003**, *321*, *3*, 147−156. https://doi.org/10.1016/S0022-3093(03)00160-1.
34. Koroleva, O.N.; Shtenberg, M.V.; Zainullina, R.T.; Lebedeva, S.M.; Nevolina, L.A. Vibrational Spectroscopy and Density of K_2O−B_2O_3−GeO_2 Glasses with Variable B/Ge Ratio. *Phys. Chem. Chem. Phys*. **2019**, *21*, *23*, 12676−12684. https://doi.org/10.1039/C9CP01374A.
35. Yiannopoulos, Y.D.; Chryssikos, G.D.; Kamitsos, E.I. Structure and properties of alkaline earth borate glasses. *Phys. Chem. glasses*. **2001**, *42*, *3*, 164–172.
36. Knoblochova, K.; Ticha, H.; Schwarz, J.; Tichy, L. Raman spectra and optical properties of selected Bi_2O_3–PbO–B_2O_3–GeO_2 glasses. *Opt. Mater*. **2009**, *31*, *6*, 895–898. https://doi.org/10.1016/j.optmat.2008.10.024.
37. Henderson, G.S.; Wang, H.M. Germanium coordination and the germanate anomaly. *Eur. J. of Mineral.* **2002**, *14*, *4*, 733-744. https://doi.org/10.1127/0935-1221/2002/0014-0733.
38. Kamitsos, E.I.; Yiannopoulos Y.D.; Karakassides, M.A.; Chryssikos, G.D.; Jain, H. Raman and infrared structural investigation of $xRb_2O{\cdot}(1-x)GeO_2$ glasses. *J. Phys. Chem*. **1996**, *100*, 11755–11765. https://doi.org/10.1364/OE.22.015924.

39. Fan, H.; Gao, G.; Wang, G.; Hu, L. Infrared, Raman and XPS spectroscopic studies of Bi_2O_3–B_2O_3–GeO_2 glasses. *Solid State Sci*. **2010**, *12*, 4, 541–545. https://doi.org/10.1016/j.solidstatesciences.2009.09.007.
40. Błaszczak, K.; Adamczyk, A.; Wędzikowska, M.; Rokita, M. Infrared studies of devitrification $Li_2O{\cdot}B_2O_3{\cdot}2GeO_2$ glass. *J. Mol. Struct*. **2004**, *704, 1-3*, 275–279. https://doi.org/10.1016/j.molstruc.2004.01.060.
41. Taqiullah, S. M.; Alshahrani, T.; Shariq, M.; Hakami, J.; Ahmad, N.; Alshehri, A. M.; Chaudhary, A.A.; Khan, S.M.; Shinde, S.M.; Slimani, Y.; Ansari, A.R.; Siddiqui, M.A.; Imran, M.;Khan, F. Utilization of infrared, Raman spectroscopy for structural analysis of alkali boro-germanate glasses. *J. Taibah Univ. Sci*. **2022**, *16, 1*, 820–827. https://doi.org/10.1021/acs.jpcc.0c07810.
42. Bolundut, L.; Pop, L.; Bosca, M.; Borodi, G.; Olar, L.; Suciu, R.C.; Pascuta, P.; Culea, E.; Stefan, R. Structural and spectroscopic properties of some neodymium-boro-germanate glasses and glass ceramics embedded with silver nanoparticles. *Cer. Int*. **2017**, *43, 15*, 12232–12238. https://doi.org/10.1016/j.ceramint.2017.06.084.
43. Morassuti, C.Y.; Nunes, L.A.; Lima, S.M.; Andrade, L.H. Eu^{3+}-doped alumino-phosphate glass for ratiometric thermometer based on the excited state absorption. *J. Lumin*. **2018**, *193*, 39–43. https://doi.org/10.1016/j.jlumin.2017.09.001.
44. Wantana, N.; Kaewjaeng, S.; Kothan, S.; Kim, H.J.; Kaewkhao, J. Energy transfer from Gd^{3+} to Sm^{3+} and luminescence characteristics of CaO–Gd_2O_3–SiO_2–B_2O_3 scintillating glasses. *J. Lumin*. **2017**, *181*, 382–386. https://doi.org/10.1016/j.jlumin.2016.09.050.
45. Meng, X.G.; Qiu, J.R.; Peng, M.Y.; Chen, D.P.; Zhao, Q.Z.; Jiang, X.W.; Zhu, C.S. Near infrared broadband emission of bismuth-doped aluminophosphate glass. *J. Opt. Express*. **2005**, *13*, 1635–1642. https://doi.org/10.1364/opex.13.001628.
46. Jaiswal, V. V.; Bishnoi, S.; Swati, G.; Singh, P.; Lohia, N.; Bathula, S.; Haranath, D. Luminescence properties of yttrium gadolinium orthovanadate nanophosphors and efficient energy transfer from VO_4^{3-} to Sm^{3+} via Gd^{3+} ions. *Arabian Journal of Chemistry*. **2020**, *13*, 474-480. https://doi.org/10.1016/j.arabjc.2017.05.020.
47. Kaczkan, M.; Boruc, Z.; Turczyński, S.; Malinowski, M. Effect of temperature on the luminescence of Sm^{3+} ions in YAM crystals. *J. Alloys Compd*. **2014**, *612*, 149–153. http://dx.doi.org/10.1016/j.jallcom.2014.05.186.
48. Pritula, I.; Gayvoronsky, V.; Gromov, Y.; Kopylovsky, M.; Kolybaeva, M.; Puzikov, V.; Kosinova, A.; Savvin, Y.; Velikhov, Y.; Levchenko, A. Linear and nonlinear optical properties of dye-doped KDP crystals: Effect of thermal treatment. *Opt. Commun*. **2009**, *15, 282, 6*, 1141–1147. https://doi.org/10.1016/j.optcom.2008.11.043.
49. Padlyak, B.; Ryba-Romanowski, W.; Lisiecki, R.; Adamiv, V.; Burak, Y.; Teslyuk, I.; Banaszak-Piechowska A. Optical spectra and luminescence kinetics of the Sm^{3+} and Yb^{3+} centres in the lithium tetraborate glasses. *Optica Applicata*. **2010**, *XL*, *2*, 427-438.
50. Kirdsiri, K.; Raja Ramakrishna, R.; Damdee, B.; Kim, H. J.; Kaewjaeng, S.; Kothan, S.; Kaewkhao, J. Investigations of optical and luminescence features of Sm^{3+} doped Li_2O-MO-B_2O_3 (M =Mg/Ca/Sr/Ba) glasses mixed with different modifier oxides as an orange light emitting phosphor for WLED's. *Journal of Alloys and Compounds*. **2018**, *749*, 197–204. https://doi.org/10.1016/j.jallcom.2018.03.266.
51. Khan, I.; Rooh, G.; Rajaramakrishna, R.; Sirsittipokakun, N.; Kim, H. J.; Ruangtaweep, Y.; Kaewkhao, J. Spectroscopy Study of Sm^{3+} Doped Fluorosilicate Glasses for Orange Emission Solid-State Device Application. *Glass Physics and Chemistry*. **2019**, *45*, *6*, 447–458. https://doi.org/10.1134/s1087659619060105.
52. Ivanova, A.A.; Gontcharenko, V.E.; Lunev, A.M.; Sidoruk, A.V.; Arkhipov, I.A.; Taydakov, I.V.; Belousov, Y.A. New Carboxylate Anionic Sm-MOF: Synthesis, Structure and Effect of the Isomorphic Substitution of Sm^{3+} with Gd^{3+} and Tb^{3+} Ions on the Luminescent Properties. *Inorganics*, **2022**, *10*, 104. https://doi.org/10.3390/inorganics10080104.